



A novel and green synthesis of mixed phase CoO@Co₃O₄@C anode material for lithium ion batteries

Halil Şahan¹ · Hüseyin Göktepe³ · Süleyman Yıldız^{2,3} · Cafer Çaymaz³ · Şaban Patat^{2,3}

Received: 2 May 2018 / Revised: 24 July 2018 / Accepted: 1 August 2018 / Published online: 9 August 2018
© Springer-Verlag GmbH Germany, part of Springer Nature 2018

Abstract

CoO composite materials had attracted wide attention due to their potential application in lithium ion batteries (LIBs). We report a green and novel solution method for making pristine Co₃O₄ and mixed phase CoO@Co₃O₄@C composite anode electrodes in LIBs. The anode materials characterized by X-ray diffraction (XRD) and scanning electron microscopy (SEM). The XRD diffraction pattern reveals that composite anode contains as a major phase of CoO and small amounts of cubic Co₃O₄ and Co metal peaks are found as impurity phases. The SEM micrographs showed that CoO, Co₃O₄, and Co phases are distributed in amorphous carbon network. The electrochemical behavior of anodes material is investigated by galvanostatic discharge/charge measurements and cyclic voltammetry. The composite anode shows a reversible specific capacity approaching 447 ± 5 mAh g⁻¹ after 10 cycles at 100 and 107 ± 5 mAh g⁻¹ after 50 cycles at 500 mA g⁻¹ as well as improved cyclic stability and excellent rate capability. The enhancement of the electrochemical performance is attributed to the good electric contact between the particles, easier lithium ion diffusion, and suppression of volume change of anode.

Keywords Lithium ion batteries · CoO · Anode materials · Capacity fade · Green synthesis · Electrochemical performance

Introduction

Designing electrode materials with high lithium storage capacity, rate capability, and long cycling life is still a major challenge for developing high-performance lithium-ion batteries (LIBs). Graphite is currently used as the anode material for commercial LIBs, but its capacity is limited to a theoretical value (372 mAh g⁻¹) and a potential of 0.1 V relative to Li/Li⁺. Recently, much effort has been focused on new anode materials with both larger capacities and slightly more positive insertion voltages with respect to Li/Li⁺ in order to minimize any risks of high-surface-area Li plating at the end of a fast

recharge [1]. Various new high-performance anode materials have been intensively investigated for next-generation LIBs [2–5]. One of the most promising classes of anode materials are conversion transition metal oxides (MOs). These MOs rely on chemical transformations with more than one electron transfer step to store and deliver energy, which results in theoretical capacities of two to three times higher than graphite. In addition, they have a safer lithiation potential that eliminates the possibility for problematic lithium plating during charging. Lastly, MOs are naturally abundant and typically environmentally friendly. However, the use of metal oxides in their raw state has been limited by their low electronic conductivity which promotes phase separation and large domain sizes from the metal and Li₂O phases that form during charging. It is this nanoscale phenomenon that limits MO cycle life compared to graphite [6]. In recent years, transition metal oxides such as CoO/Co₃O₄ [7–13], MoO₃ [13, 14], SnO₂ [13–15], NiO [13, 16, 17], and ZnO [13, 18], NiFe₂O₄ [13, 19] have shown promising applications in lithium ion battery due to their high theoretical capacity and high abundance.

The anodic properties of Co₃O₄ and CoO were first reported by Poizot et al. in year 2000 [20]. Among the transition metal oxides, cobalt monoxide (CoO) is considered as an ideal

✉ Halil Şahan
halilsahan77@gmail.com

¹ Center for Renewable Energy Technology, Department of Chemistry and Chemical Biology, Northeastern University, Boston, MA 02115, USA

² Science Faculty, Department of Chemistry, Erciyes University, Kayseri, Turkey

³ Erciyes University, Nanotechnology Research Center, Kayseri, Turkey

anode material for LIBs owing to its high theoretical Li-ion storage capacity of 715 mAh g^{-1} , whose completely reversible electrochemical reaction is as follows [21] $\text{CoO} + 2\text{Li}^+ + 2\text{e}^- \leftrightarrow \text{Co} + \text{Li}_2\text{O}$.

Nevertheless, the utilization of CoO is hindered by its poor electronic conductivity and capacity retention and poor cycling stability due to the large volume changes and stresses during the lithium ion insertion/extraction processes, which result in insignificant capacity fading [22]. In order to overcome these barriers, many appealing strategies have been adopted to ameliorate the electrochemical performances of CoO. To overcome these difficulties, compositing with carbon materials such as graphene or carbon nanotubes has been proven to be an effective strategy to improve the Li-ion storage capability of CoO anodes. All of these works [23, 24] made a great contribution to enhance the CoO anode for LIBs. However, other new composite systems with low cost and facile preparation are an urgent need for practical application of Li-ion batteries. Amorphous carbon is a common conductive additive usually applied to the preparation of composite anode electrode. It presents both an amorphous microstructure with excellent ability to improve the conductivity between the electrode and binder materials and suppression of the enlargement of particle size.

In literature, Co_3O_4 has been extensively investigated as an anode material, because this material can be easy to prepare in comparison to CoO or Co_2O_3 . To improve electrochemical performance of cobalt oxide anode materials, different synthesis methods were applied. It can be easily prepared by various conventional methods such as the solid state method, hydrothermal method [25], precipitation [26], virus-enabled synthesis [27], template method [28], ammonia-evaporation-induced method [29], molten salt method [30], thermal decomposition [31], physical methods [13, 32], etc.

For example, Reddy et al. synthesized Co_3O_4 compounds using different molten salts. They reported the growth, reaction mechanism, and lithium storage performance of different Co_3O_4 [33]. To prepare Co_3O_4 , and CoO, the urea combustion method and carbothermal reduction methods were adopted by Reddy et al. These compounds were prepared in the form of nano-rod/particles and investigated the Li-cycling properties, and their use as an anode material [34].

In this study, we first prepared mixed phase $\text{CoO@Co}_3\text{O}_4\text{@C}$ via *Punica granatum* extract which acts as both the reducing agent and the carbon source. This process produces mixed metal oxide particles by the self-generated heat of reaction in a very short reaction time. *Punica granatum* extract is rich in sugar (fructose and glucose) that can function as reductants and presumably can be responsible to modify size and morphology. The present synthesis is very helpful to produce highly crystalline sub-micron size particles with distinctive shape and good electrical conductivity between the

particles, which exhibit promise for application as an anode material in LIBs.

Experimental

Extraction procedure

Punica granatum shells were dried at 100°C for an overnight in air atmosphere. The dry shells were suspended in 100 mL ultra pure water. This suspension refluxed at 150°C for 1 h. Finally, the red suspension centrifuged at 4000 and 16,000 rpm for 15 min and then stored at 4°C .

Synthesis of $\text{CoO@Co}_3\text{O}_4\text{@C}$ anode material

In a typical synthesis process, stoichiometric amount of cobalt acetate was mixed with 3 mL *Punica granatum* extract. This red suspension was heated in air for the evaporation of excess water. At the end of this process, the red transparent gel was obtained. Finally, this gel was annealed in a tube furnace at 400°C for 2 h in Ar atmosphere to form a porous $\text{CoO@Co}_3\text{O}_4\text{@C}$. For comparison, pristine Co_3O_4 were also synthesized under the same condition in the air, except for *Punica granatum* extract.

Characterization techniques

Thermal analysis of the precursor sample of anode material was carried out using a PerkinElmer (Diamond) TG/DTA thermal analyzer at a heating rate of 5°C min^{-1} under air and N_2 atmosphere for pristine Co_3O_4 and $\text{CoO@Co}_3\text{O}_4\text{@C}$ composite, respectively.

The crystal structures of the samples were characterized by X-ray diffractometer (Bruker D8 Advance) equipped with $\text{Cu-K}\alpha$ radiation ($\lambda = 1.54178 \text{ \AA}$) and a graphite monochromator. Scanning electron microscope (SEM, Zeiss EVO) was used to observe the morphology of the powders by equipping energy dispersive spectroscopy (EDS) to the performed element composition of the powders.

Electrochemical measurements

The electrode slurry was fabricated by mixing active materials with polyvinylidene fluoride (PVDF was dissolved in *N*-methyl-2-pyrrolidone (NMP) with a content of 10 wt%) as a binder and Super P carbon black as a conductive agent with a weight ratio of 8:1:1. This slurry was coated onto Cu foils via doctor blade technique and then dried at 120°C for overnight in a vacuum oven. Each electrode was cut into discs with diameter of 11 mm. The final working electrodes were usually discs whose active masses exposed to the electrolyte solution were $4\text{--}5 \text{ mg cm}^{-2}$. Electrochemical measurements were

performed using Swagelok-type cells with lithium foil as the counter/reference electrode, glass microfiber filters (Whatman) as the separator. The electrolyte was a 1 M LiPF_6 solution in a 50:50 (w/w) mixture of ethylene carbonate (EC) and diethyl carbonate (DEC). The cells were assembled in argon-filled MBraun Uni Lab glovebox. All the as-prepared cells were stabilized for 5 h before the measurements. The cells were galvanostatically charged and discharged on an 8-channel MTI battery analyzer. The electrode capacity was measured by a galvanostatic discharge-charge method in the voltage range between 0.01 and 3.0 V at various current densities of 100 to 500 mA g^{-1} on a battery test system. Cyclic voltammogram (CV) measurements were performed with a VersaSTAT MC multi-channel potentiostat/galvanostat/impedance analyzer. CV tests were examined in the voltage range of 0.01–3 V at scan rate 0.1 mV s^{-1} . Electronic conductivity of anodes was measured by linear scanning voltammetry method with a VersaSTAT MC multi-channel potentiostat/galvanostat/impedance analyzer.

Results and discussion

Figure 1 shows TG analysis of pristine Co_3O_4 and $\text{CoO}@/\text{Co}_3\text{O}_4@\text{C}$ composite. The TG analysis of cobalt acetate with *Punica granatum* extract and pristine cobalt acetate was figured out in N_2 and air atmosphere, respectively. TG analysis showed that two curves resemble each other. It is evident from the TG curve that decomposition occurs in three steps. First step is that of the dehydration in which four water molecules are eliminated in temperature range of 40–120 $^\circ\text{C}$. At temperature range of 180–260 $^\circ\text{C}$, anhydrous cobalt acetate decomposes to yield acetone as volatile and cobalt carbonate as residue. The cobalt carbonate is unstable and decomposes to yield CoO as residue and CO_2 as volatile. This reaction occurs in 263–300 $^\circ\text{C}$. TG curve corroborates no further thermal reactions beyond 400 $^\circ\text{C}$.

The crystalline nature and composition of samples were examined by XRD. The XRD patterns of as-synthesized pristine Co_3O_4 , $\text{CoO}@/\text{Co}_3\text{O}_4@\text{C}$ composite are shown in Fig. 2. Figure 2 shows the XRD patterns of the final composite, which is in agreement with CoO, Co_3O_4 , and Co (JCPDS card no. 02-1217, no. 42-1467, no. 05-0827, respectively). No obvious peaks corresponding to crystalline carbon can be observed. However, amorphous carbon created from *Punica granatum* extract cannot be excluded. All of the diffraction peaks in this pattern are in good agreement with the standard crystallographic data for cubic CoO. In addition to the major phase of CoO, small amounts of cubic Co_3O_4 and Co metal peaks are found as impurity phases. Reddy et al. synthesized CoO from Co_3O_4 via the carbothermal method [33]. Because of Co_3O_4 used as a precursor and carbon used as a reducing agent, a unique phase of CoO is obtained

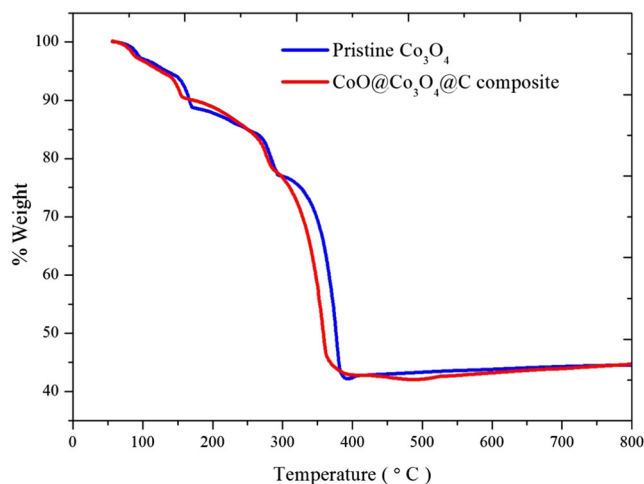


Fig. 1 Thermogravimetric analysis (TG) of precursor samples

in this carbothermal method. On the contrary of the result, because of *Punica granatum* extract mixed with cobalt acetate, we synthesized mixed phase CoO anode material which consists of Co and Co_3O_4 . Previous synthesis which is related with $\text{Co}_3\text{O}_4/\text{CoO}$ is similar to our XRD data and synthesis results [34, 35].

Lattice constants were calculated from the XRD pattern of Fig. 2 with a least-squares refinement. The lattice constants of Co_3O_4 , $\text{CoO}@/\text{Co}_3\text{O}_4@\text{C}$ composite were determined to be 8.084(2) and 4.261(3) using the Fd3m and Fm3m space group during Rietveld refinements, respectively. XRD data analysis showed that the lattice parameter values of anode materials are in good agreement with previous studies [36, 37].

The SEM images depicting the morphologies and microstructures of the materials are shown in Fig. 3. It can be seen clearly from Fig. 3a, c that the particle distribution of composite material is heterogeneous. As seen from the XRD pattern,

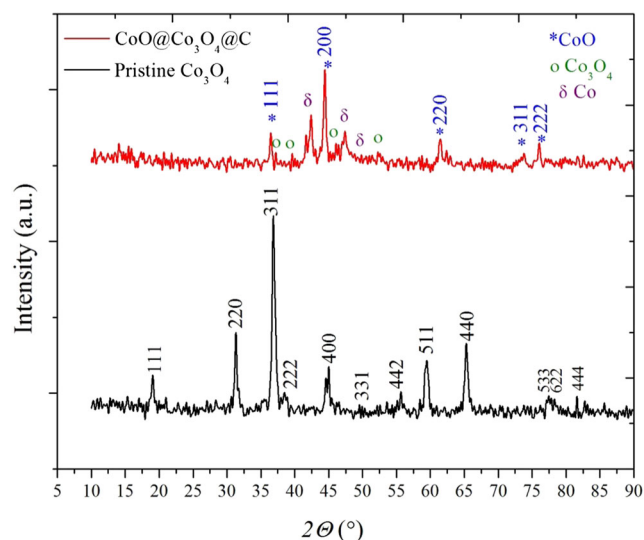
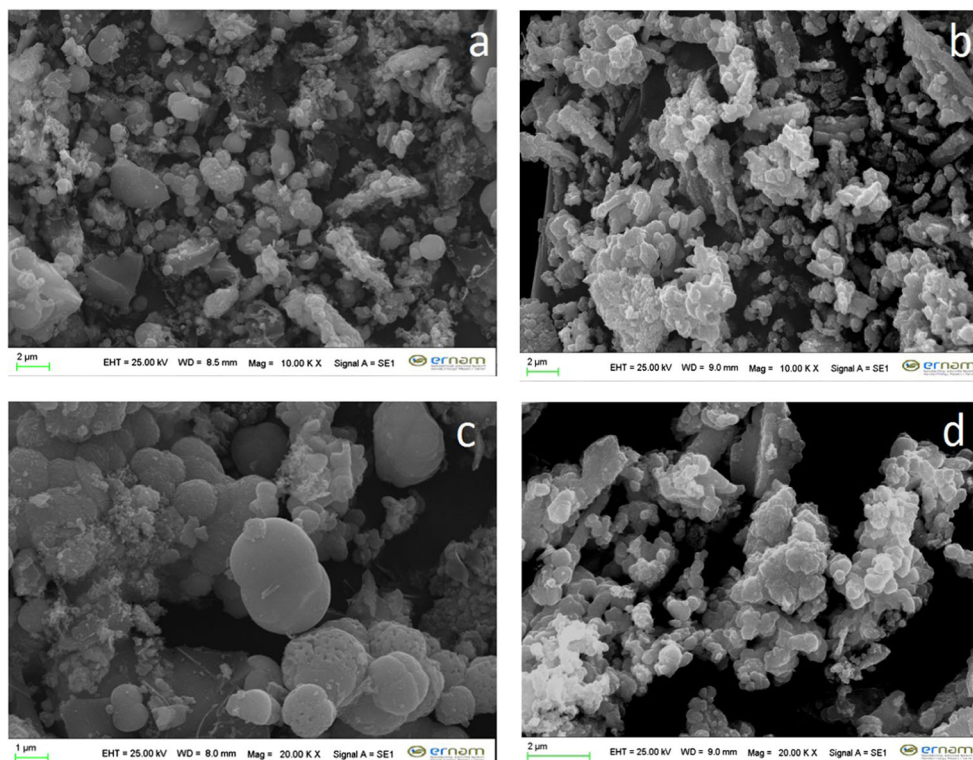


Fig. 2 XRD pattern of $\text{CoO}@/\text{Co}_3\text{O}_4@\text{C}$ composite and pristine Co_3O_4

Fig. 3 SEM images of **a, c** CoO@Co₃O₄@C composite and **b, d** pristine Co₃O₄ (low and high magnification, respectively)



three different particle morphologies are shown in Fig. 3a, c. Probably, these particles which are distributed in amorphous carbon network belong to CoO, Co₃O₄, and Co phases, respectively. In contrast to composite morphology and microstructure, particle distribution of pristine Co₃O₄ is very homogenous. As seen in Fig. 3b, d, the particles agglomerated and the particle size of pristine Co₃O₄ is between 100 and 500 nm.

Furthermore, to verify the chemical composition of the synthesized particles, the EDS analysis of sample CoO@Co₃O₄@C composite by SEM-EDS mode was conducted (Fig. 4). As shown in Fig. 4, EDS spectrum of the sample exhibits the characteristic peaks of Co, O, and C indicating the CoO@Co₃O₄@C composite phase purity in the synthesized particles. From the EDS spectrum, the Co, O, and C content in the anode material was calculated as a 57.3, 29.1, and 13.5 wt%, respectively. The characteristic peaks of Au which are seen in 2.3 and 9.8 keV in the spectrum belong to coating materials which are used in sputter coating process.

The resistance (R) was extracted from the I - V curve based on Ohm's law. Resistivity (δ) was determined using the equation $R = \delta \frac{L}{A}$ where A is the pellet area and L is its thickness. $1/\delta$ yielded the dc electronic conductivity for each cathode. Electronic conductivity of pristine Co₃O₄ and CoO@Co₃O₄@C composite was found as a 1.14E-6 S cm⁻¹ and 0.231 S cm⁻¹, respectively. The electronic conductivity results of anodes displayed that the amorphous carbon enhances the electronic conductivity by 10⁵ times.

Figure 5a, b shows the CV curves of the pristine Co₃O₄ and CoO@Co₃O₄@C composite anodes. The CV measurements were performed to determine the electrochemical reaction of the samples. It is observed that the cathodic peak in the first cycle of the pristine Co₃O₄ at about 0.6 V could be attributed to the irreversible formation of a solid electrolyte interface (SEI) film (Reaction 1) [38, 39]. The cathodic peak at 0.8 V could correspond to the formation of Li₂O and Co by the reduction of CoO (Reaction 2). In the subsequent cycles, the cathodic peak slightly shifts to a lower potential. However, one cathodic peak in the first cycle is seen at 0.47 V for the CoO@Co₃O₄@C composite anode (reaction 1 and 2). The pristine Co₃O₄ and CoO@Co₃O₄@C composite anodes of the first anodic process of the oxidation peak at about 2.1 V are assigned to the oxidation of CoO (Reaction 3 and 4), and the anodic peaks changed slightly in the second and third cycles. Even if we applied after the 20th charge-discharge at 200 mA g⁻¹, it can be seen clearly from Fig. 5b that the CV curves of CoO@Co₃O₄@C composite anode slightly shifted which is related with reversible electrochemical reaction. In contrast with this tendency, the CV curves of pristine anode separated and peak intensity decreased due to high polarization in the cell.

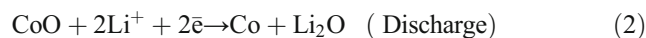
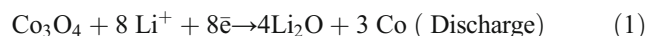


Fig. 4 EDS spectrum result of CoO@Co₃O₄@C composite

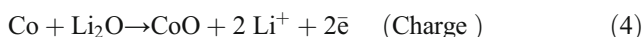
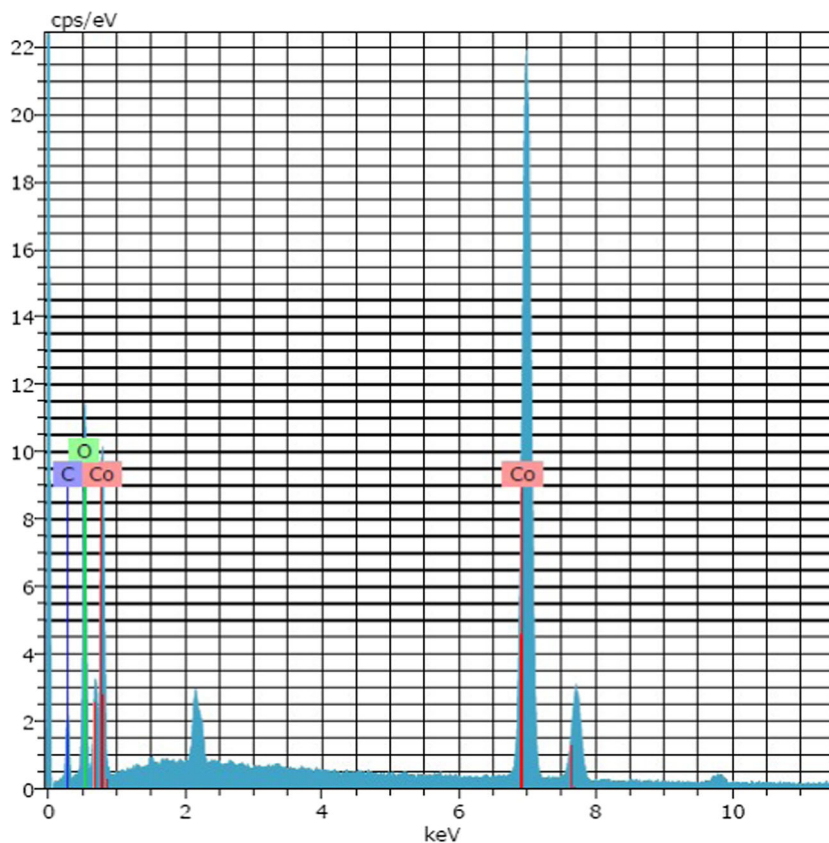


Figure 6a, b displays the galvanostatic discharge-charge curves of pristine Co₃O₄ and CoO@Co₃O₄@C composite electrode for the first, second, and 10th cycles, respectively, between 0.01 and 3.0 V at a current density of 100 mA g⁻¹. The curves of pristine Co₃O₄ and CoO@Co₃O₄@C composite electrode are well consistent with the CV curves. The voltage trends are well indicative of typical characteristics of CoO and Co₃O₄ [40]. Two sloping voltage plateaus at ca. 1.2 and 0.8 V in the discharge profiles and the voltage plateaus at ca. 1.3 and 2.2 V in the charge profiles were ascribed to the lithium insertion/extraction processes in CoO. However, it changed to a long sloping voltage plateau at 1.2 and 0.8 V that showed a gradual decay in the following charge/discharge processes, indicating some irreversible reaction during the charge/discharge processes due to the amorphous metal oxides in the pristine anode. Two potential plateaus at around 1.0 and 0.5 V in the discharge curves were observed, which can be ascribed to the reduction of Co₃O₄ to CoO and CoO to Co, respectively. Depending on the crystallite size and surface area of Co₃O₄, and the applied current, in the early stages of the first discharge (150 mAh g⁻¹ or 1.5 Li/Co₃O₄), these show

evidence of lithium intercalation into Co₃O₄, i.e., Li_xCo₃O₄ or through the conversion to Li₂O and CoO (large domains and/or high current densities) [41], which, upon further reduction, indistinctively decompose into Co and Li₂O. However, a unique path is generally observed upon oxidation of the nanometric composite, generally appearing to lead to the partial oxidation of cobalt to form CoO, which becomes the active material upon further cycling, instead of Co₃O₄ [42].

As shown in Fig. 6a, the discharge and charge capacities of pristine electrode are 1052 ± 5 and 586 ± 5 mAh g⁻¹ in the first cycle, respectively, indicating a coulombic efficiency of 55.7%. It can deliver discharge capacity of 613 ± 5 mAh g⁻¹ in the 2nd cycle, and after the 10th cycle, the discharge capacity is only 151 ± 5 mAh g⁻¹. The huge capacity fading ratio between 2nd and 10th cycle was calculated as a 75.4%. The relatively low initial coulombic efficiency may be caused by irreversible capacity loss which may arise from the formation of SEI film (irreversible reactions) in the first discharge [43, 44]. Irreversible capacity loss is common to most anode materials [45–47]. However, the CoO@Co₃O₄@C composite electrode has lower initial discharge and charge capacity which are 731 ± 5 and 472 ± 5 mAh g⁻¹, respectively, and the coulombic efficiency is 64.5%. The reason of a lower initial discharge and charge capacity of composite electrode may be related with electrochemical inactive Co metal phase in the composite. The 2nd and 10th discharge capacity of

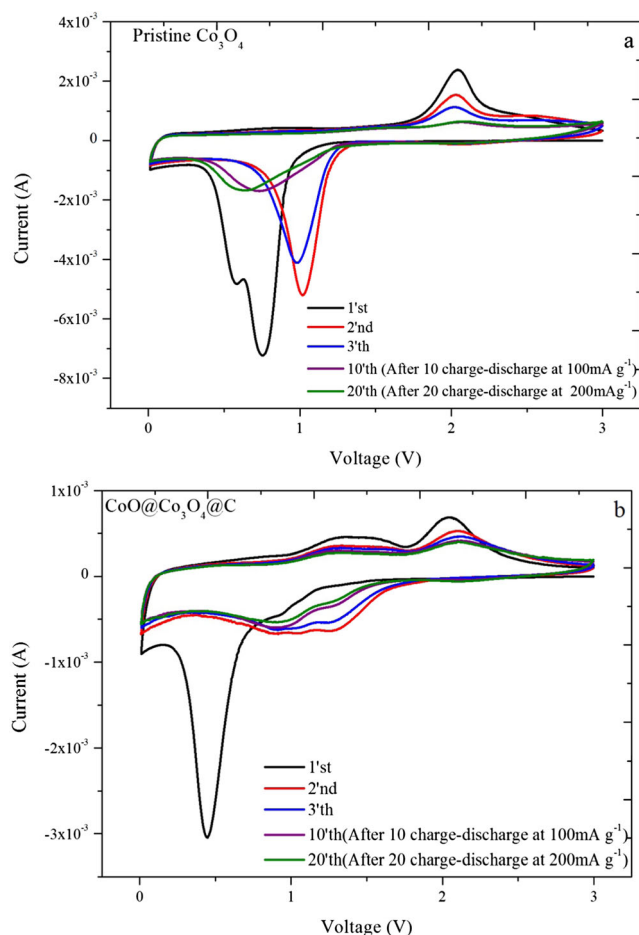


Fig. 5 Cyclic voltammograms **a** pristine Co_3O_4 and **b** $\text{CoO}@/\text{Co}_3\text{O}_4@\text{C}$ composite anode. Scan rate 0.1 mV s^{-1}

composite electrode are 473 ± 5 and $447 \pm 5 \text{ mAh g}^{-1}$, respectively. No huge capacity attenuation was observed in the process of charging/discharging. In the same condition, the capacity fading ratio was calculated as only 5%.

To further investigate the rate capacity, two samples of pristine and $\text{CoO}@/\text{Co}_3\text{O}_4@\text{C}$ composite as electrode are cycled at various current densities between 100, 200, and 500 mA g^{-1} as shown in Fig. 7. The rate capacity is one of the most critical issues with the lithium battery application. As shown in Fig. 7, the capacities of both electrodes decreased monotonically as the rate increased, while the $\text{CoO}@/\text{Co}_3\text{O}_4@\text{C}$ composite electrode exhibited a much higher capacity at a higher rate. The $\text{CoO}@/\text{Co}_3\text{O}_4@\text{C}$ composite anode delivered capacities up to 473 ± 5 , 373 ± 5 , and $158 \pm 5 \text{ mAh g}^{-1}$ at high current densities of 100, 200, and 500 mA g^{-1} respectively, which is corresponding to 93.9% (After 10th cycle), 76.4% (After 30th cycle), and 67.8% (After 50th cycle) retention of the capacity. In addition, when the current density recovered to 100 mA g^{-1} , it could restore a relatively stable capacity of $\sim 318 \pm 5 \text{ mAh g}^{-1}$. However, the pristine Co_3O_4 electrode only exhibited the rate capacities of 613 ± 5 , 121 ± 5 , and $50 \pm 5 \text{ mAh g}^{-1}$ at the 100,

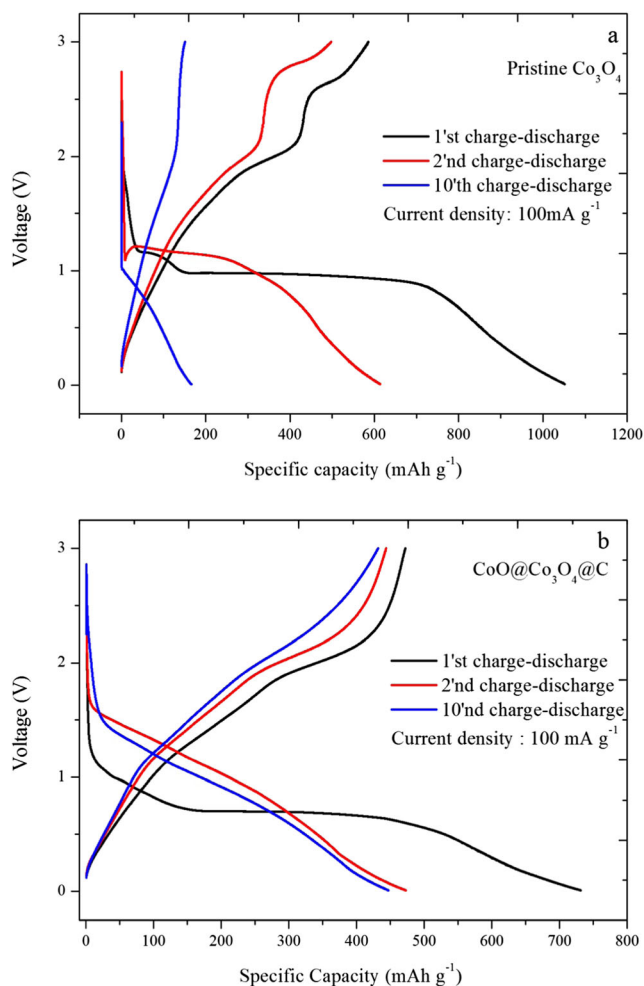


Fig. 6 First charge-discharge curves of **a** pristine Co_3O_4 and **b** $\text{CoO}@/\text{Co}_3\text{O}_4@\text{C}$ composite anode materials in the potential range of 0.01–3 V. Two-electrode swagelok-type cells, EC–DEC 1:1/1 M LiPF_6 solutions

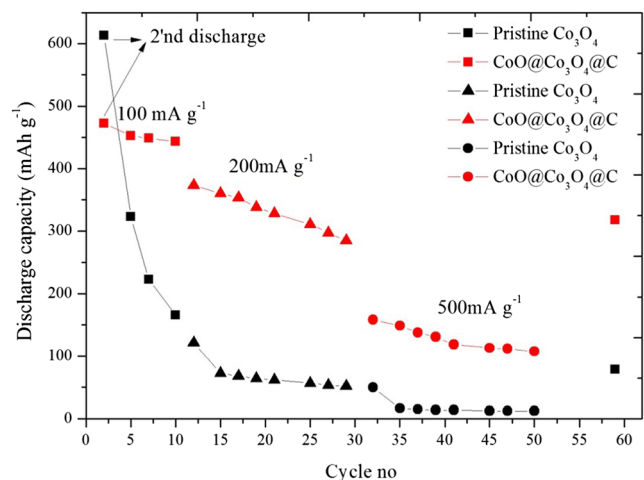


Fig. 7 Rate performance of pristine Co_3O_4 and $\text{CoO}@/\text{Co}_3\text{O}_4@\text{C}$ composite anodes in the potential range of 0.01–3 V. Two electrode swagelok-type cells, EC–DEC 1:1/1 M LiPF_6 solutions

200, and 500 mA g⁻¹, respectively. When the current density returns to 100 mA g⁻¹, the pristine electrode cannot regain its initial capacity back. Only 13% (~ 80 mAh g⁻¹) of its capacity is recovered.

According to the results presented above, the significantly improved rate capability and cycle-ability of the CoO@Co₃O₄@C composite electrode may be attributed to two main factors. First, the pristine cobalt oxide electrode suffered from large initial irreversible loss, low capacity retention upon cycling, and poor rate capability, due to the poor electronic conductivity and large volume changes during repeated lithiation/delithiation reactions [13, 48, 49]. However, due to the fact that composite electrode contains 13.5% *w/w* amorphous carbon and cobalt metal, its electronic conductivity is bigger than the pristine one. The amorphous carbon which is the best economical carbon source efficiently buffers the volume change of metal oxides during charge/discharge processes and enhances the electrical conductivity of cobalt oxide. Second, according to the literature, solid-electrolyte interphase is a principal factor in irreversible capacity loss during the initial few cycles because the formation of SEI consumes Li ions [50]. Irreversible capacity loss (ICL) occurs in many reasons: nature of crystal structure, particle size [51–54], and reduction of solvent in the electrolyte. Thus, this process is difficult to avoid. An unstable and thick SEI layer ultimately results in high internal resistance and low coulombic efficiency (defined as the efficiency of electrons transferring in an electrochemical reaction, usually the ratio of lithiation capacity to delithiation capacity). A low coulombic efficiency at the first cycle is ascribed to the formation of SEI [55, 56]. For high-performance batteries, the SEI layer should be electronically resistive to avoid SEI thickening and ionically conductive to reduce overvoltage [57]. The amorphous carbon may contribute to the growth of certain thickness of solid electrolyte interface (SEI). This is very challenging and has not been effectively addressed for materials undergoing large volume changes. Electrolyte decomposition occurs due to the low potential of the anode and forms a passivating SEI layer on the electrode surface during battery charging [58, 59]. The absence of stable solid electrolyte interface (SEI) film results in a rapid capacity fading due to continuous electrolyte decomposition [60, 61].

As a result, owing to the synergistic effect from the carbon coating layer, it was observed that Li-storage performance of the CoO@Co₃O₄@C composite electrode could be enhanced to a great extent, especially at a higher rate condition.

Conclusions

We demonstrated that a novel and green synthesis method can be used to fabricate CoO composite anodes for LIBs. CoO@Co₃O₄@C composite electrode exhibits a higher specific capacity than pristine Co₃O₄ and superior cyclability. At

a current density of 200 mA g⁻¹, the CoO@Co₃O₄@C composite anode keeps a discharge capacity of 285 ± 5 mAh g⁻¹ and 76.4% discharge capacity retention during the 30th cycle. At 500 mA g⁻¹, composite anode still presents a discharge capacity of 108 ± 5 mAh g⁻¹ and 97.4% coulombic efficiency during the 50th cycle. The green-novel strategy is simple and low cost and promising for mass production, and the remarkable electrochemical performance demonstrates that the CoO@Co₃O₄@C composite anode has potential applications in high-performance LIBs.

References

1. Tarascon JM, Armand M (2001) Issues and challenges facing rechargeable lithium batteries. *Nature* 414:359–367
2. Yan N, Hu L, Li Y, Wang Y, Zhong H, Hu X, Kong X, Chen Q (2012) Co₃O₄ nanocages for high-performance anode material in lithium-ion batteries. *J Phys Chem C* 116(12):7227–7235
3. Derrien G, Hassoun J, Panero S, Scrosati B (2007) Nanostructured Sn–C composite as an advanced anode material in high-performance lithium-ion batteries. *Adv Mater* 19:2336–2340
4. Xiang J, Tu J, Huang X, Yang Y (2008) A comparison of anodically grown CuO nanotube film and Cu₂O film as anodes for lithium ion batteries. *J Solid State Electrochem* 12:941–945
5. Pan Q, Liu J (2009) Facile fabrication of porous NiO films for lithium-ion batteries with high reversibility and rate capability. *J Solid State Electrochem* 13:1591–1597
6. Spinner JN, Zhang V, Mustain W (2014) Investigation of metal oxide anode degradation in lithium-ion batteries *via* identical-location TEM. *J Mater Chem A* 2:1627–1630
7. Wu FD, Wang Y (2011) Self-assembled echinus-like nanostructures of mesoporous CoO nanorod@CNT for lithium-ion batteries. *J Mater Chem* 21:6636–6641
8. Sun YM, Hu XL, Luo X, Huang YH (2012) Ultrathin CoO/graphene hybrid nanosheets: a highly stable anode material for lithium-ion batteries. *J Phys Chem C* 116:20794–20799
9. Yao WL, Yang J, Wang JL, Tao LA (2008) Synthesis and electrochemical performance of carbon nanofiber-cobalt oxide composites. *Electrochim Acta* 53:7326–7330
10. Yao WL, Yang J, Wang JL, Nuli Y (2008) Multilayered cobalt oxide platelets for negative electrode material of a lithium-ion battery. *J Electrochem Soc* 155:H903–H908
11. Wang GX, Chen Y, Konstantinov K, Lindsay M, Liu HK, Dou SX (2002) Investigation of cobalt oxides as anode materials for Li-ion batteries. *J Power Sources* 109:142–147
12. Tummala R, Guduru RK, Mohanty PS (2012) Binder free, porous and nanostructured Co₃O₄ anode for Li-ion batteries from solution precursor plasma deposition. *J Power Sources* 199:270–277
13. Reddy MV, SubbaRao GV, Chowdari BVR (2013) Metal oxides and oxysalts as anode materials for Li ion batteries. *Chem Rev* 113:5364–5457
14. Wang ZY, Madhavi S, Lou XV (2012) Ultralong alpha-MoO₃ nanobelts: synthesis and effect of binder choice on their lithium storage properties. *J Phys Chem C* 116:12508–12513
15. Guo H, Mao R, Yang XJ, Wang SX, Chen J (2012) Hollow nanotubular SnO₂ with improved lithium storage. *J Power Sources* 219:280–284
16. Xie D, Yuan WW, Dong ZM, Su QM, Zhang J, Du HG (2013) Facile synthesis of porous NiO hollow microspheres and its

- electrochemical lithium-storage performance. *Electrochim Acta* 92: 87–92
17. Zhang GH, Chen YJ, Qu BH, Hu LL, Mei L, Lei DN, Li Q, Chen LB, Li OH, Wang TH (2012) Synthesis of mesoporous NiO nanospheres as anode materials for lithium ion batteries. *Electrochim Acta* 80:140–147
 18. Zhou YN, Li VX, Fu ZV (2012) Electrochemical reactivity of nanocomposite ZnO-Se for lithium-ion batteries. *Electrochim Acta* 59:435–440
 19. Cherian CT, Sundaramurthy J, Reddy MV, Kumar PS, Mani K, Pliszka D, Sow SM, Chowdari BVR (2013) Morphologically robust NiFe₂O₄ nanofibers as high capacity Li-ion battery anode material. *ACS App Mater Interfaces* 5(20):9957–9963
 20. Poizat P, Laruelle S, Grugeon S, Dupont L, Tarascon JM (2000) Nano-sized transition-metal oxides as negative-electrode materials for lithium-ion batteries. *Nature* 407(6803):496–499
 21. Zhang M, Jia MQ, Jin YH, Shi XR (2012) Synthesis and electrochemical performance of CoO/graphene nanocomposite as anode for lithium ion batteries. *App Surf Sci* 263:573–578
 22. Peng CX, Chen BD, Qin Y, Yang SH, Li CZ, Zuo YH, Liu SY, Yang JH (2012) Facile ultrasonic synthesis of CoO quantum dot/graphene nanosheet composites with high lithium storage capacity. *ACS Nano* 6:1074–1081
 23. Wu ZS, Ren WC, Wen L, Gao LB, Zhao JP, Chen ZP, Zhou GM, Li F, Cheng LM (2010) Graphene anchored with Co₃O₄ nanoparticles as anode of lithium ion batteries with enhanced reversible capacity and cyclic performance. *ACS Nano* 4:3187–3194
 24. Zhang M, Uchaker E, Hu S, Zhang Q, Wang T, Cao G, Li J (2013) CoO-carbon nanofiber networks prepared by electrospinning as binder-free anode materials for lithium-ion batteries with enhanced properties. *Nanoscale* 5:12342–12349
 25. Huang H, Zhu W, Tao X, Xia Y, Yu Z, Fang J, Gan Y, Zhang W (2012) Nanocrystal-constructed mesoporous single-crystalline Co₃O₄ nanobelts with superior rate capability for advanced lithium-ion batteries. *ACS Appl Mater Interfaces* 4(11):5974–5980
 26. Binotto G, Larcher D, Prakash AS, Hegde MS, Tarascon JM (2007) Synthesis, characterization, and Li-electrochemical performance of highly porous Co₃O₄ powders. *Chem Mater* 19(12):3032–3040
 27. Nam KT, Kim DW, Yoo PJ, Chiang CY, Meethong N, Hammond PT, Chiang YM (2006) Virus-enabled synthesis and assembly of nanowires for lithium ion battery electrodes. *Science* 312(5775): 885–888
 28. Li WY, Xu LN, Chen J (2005) Co₃O₄ nanomaterials in lithium-ion batteries and gas sensors. *Adv Funct Mater* 15:851–857
 29. Li YG, Wu Y (2010) Critical role of screw dislocation in the growth of co(OH)₂ nanowires as intermediates for Co₃O₄ nanowire growth. *Chem Mater* 22(19):5537–5542
 30. Reddy MV, Beichen Z, Loh KP, Chowdari BVR (2013) Facile synthesis of Co₃O₄ by molten salt method and its Li-storage performance. *Cryst Eng Comm* 15:3568–3574
 31. Yang R, Wang Z, Liu J, Chen L (2004) Nano Co₃O₄ particles embedded in porous hard carbon spherules as anode material for Li-ion batteries. *Solid State Lett* 7:A496–A499
 32. Varghese B, Teo CH, Zhu Y, Reddy MV, Chowdari VR, Wee AT, Tan BC, Lim CT, Sow CH (2007) Co₃O₄ nanostructures with different morphologies and their field-emission properties. *Adv Funct Mater* 17:1932–1939
 33. Reddy MV, Beichen Z, Nicholette LJ, Kaimenga Z, Chowdaria BVR (2011) Molten salt synthesis and its electrochemical characterization of Co₃O₄ for lithium batteries. *Electrochem Solid State Lett* 14(5):A79–A82
 34. Reddy MV, Prithvi Loh KP, Chowdari BVR (2014) Li storage and impedance spectroscopy studies on Co₃O₄, CoO, and CoN for Li-ion batteries. *ACS Appl Mater Interfaces* 6:680–690
 35. Yao W, Chen J, Cheng H (2011) Platelike CoO/carbon nanofiber composite electrode with improved electrochemical performance for lithium ion batteries. *J Solid State Electrochem* 15:183–188
 36. Berenguer R, Valdés-Solis T, Fuertes AB, Quijada C, Morallón E (2008) Cyanide and phenol oxidation on nanostructured Co₃O₄ electrodes prepared by different methods. *J Electrochem Soc* 155(7): K110–K115
 37. Yang HM, Ouyang J, Tang AD (2007) Single step synthesis of high-purity CoO nanocrystals. *J Phys Chem B* 111:8006–8013
 38. Pramanik A, Maiti S, Sreemany S (2016) Electrochemical energy storage in self-assembled nest-like CoO nanofibers with long cycle life. *J Nanopart Res* 18:93–105
 39. Chen C, Huang M, Zhang H, Wang X, Wang Y, Jiao L, Yuan H (2016) Controllable synthesis of Cu-doped CoO hierarchical structure for high performance lithium-ion battery. *J Power Sources* 314: 66–75
 40. Zhang Y, Li Y, Chen J, Zhao P, Li D, Mu J, Zhang L (2017) CoO/Co₃O₄/graphene nanocomposites as anode materials for lithium-ion batteries. *J Alloys Comp* 699:672–678
 41. Larcher D, Sudant G, Leriche JB, Chabre Y, Tarascon JM (2002) The electrochemical reduction of Co₃O₄ in a lithium cell. *J Electrochem Soc* 149:A234–A241
 42. WenFu Z, Wang Y, Zhang Y, Qin QZ (2004) Electrochemical reaction of nanocrystalline Co₃O₄ thin film with lithium. *Solid State Ionics* 170(1):105–109
 43. Kim Y, Kim S (2015) Direct growth of cobalt aluminum double hydroxides on graphene nanosheets and the capacitive properties of resulting composites. *Electrochim Acta* 163:252–259
 44. Wu JF, Zuo LYH, Song YH, Chen YQ, Zhou RH, Chen SH, Wang L (2016) Preparation of biomass-derived hierarchically porous carbon/Co₃O₄ nanocomposites as anode materials for lithium-ion batteries. *J Alloys Compd* 656:745–752
 45. He J, Wu S, Zhao NQ, Shi CS, Liu CS, Li JJ (2013) Carbon-encapsulated Fe₃O₄ nanoparticles as a high-rate lithium ion battery anode material. *ACS Nano* 7:4459–4469
 46. Lv WM, Zhao J, Wen FS, Xiang JY, Li L, Wang LM, Liu ZY, Tian YJ (2015) Carbonaceous photonic crystals as ultralong cycling anodes for lithium and sodium batteries. *J Mater Chem A* 3:13786–13793
 47. Chang K, Chen WX (2011) L-Cysteine-assisted synthesis of layered MoS₂/graphene composites with excellent electrochemical performances for lithium ion batteries. *ACS Nano* 5:4720–4728
 48. Jiang J, Li LL, Liu JP, Huang XT, Yuan CZ, Lou XW (2012) Recent advances in metal oxide-based electrode architecture design for electrochemical energy storage. *Adv Mater* 24:5166–5180
 49. Geng H, Guo Y, Ding X, Wang H, Zhang Y, Wu X, Jiang J, Zheng J, Yang Y, Gu H (2016) Porous cubes constructed by cobalt oxide nanocrystals with graphene sheet coatings for enhanced lithium storage properties. *Nanoscale* 8: 7688–7694
 50. Ji G, Ma Y, Lee JY (2011) Mitigating the initial capacity loss (ICL) problem in high capacity lithium ion battery anode materials. *J Mater Chem* 21(27):9819–9824
 51. Reddy MV, Yu C, Jiahuan F, Loh KP, Chowdari BVR (2013) Li-cycling properties of molten salt method prepared nano/submicrometer and micrometer-sized CuO for lithium batteries. *ACS Applied Mater Inter* 5(10):4361–4366
 52. Reddy MV, Wen BLW, Loh KP, Chowdar BVR (2013) Energy storage studies on InVO₄ as high performance anode material for Li-ion batteries. *ACS Applied Mater Inter* 5(16):7777–7785
 53. Ramasami AK, Reddy MV, Balakrishna GR (2015) Combustion synthesis and characterization of NiO nanoparticles. *Mater Sci Semicond Process* 40: 194–202
 54. Reddy MV, Andreea LYT, Ling AY, Hwee JNC, Lin CA (2013) Effect of preparation temperature and cycling voltage range on molten salt method prepared SnO₂. *Electrochim Acta* 106:143–148

55. Ma GY, Lee JY (2011) Mitigating the initial capacity loss (ICL) problem in high capacity lithium ion battery anode materials. *J Mater Chem* 21(27):9819–9824
56. Wu H, Chan G, Choi JW, Ryu I, Yao Y (2012) Stable cycling of double-walled silicon nanotube battery anodes through solid-electrolyte interphase control. *Nat Nanotechnol* 7(5):310–315
57. Mogensen KB, Gangloff L, Boggild P, Teo KBK, Milne WI, Kutter JP (2009) N carbon nanotubes integrated in electrically insulated channels for lab-on-a-chip applications. *Nanotechnology* 20(9):095503
58. Aurbach D (2000) Review of selected electrode–solution interactions which determine the performance of Li and Li ion batteries. *J Power Sources* 89:206–218
59. Verma P, Maire P, Novak P (2010) A review of the features and analyses of the solid electrolyte interphase in Li-ion batteries. *Electrochim Acta* 55:6332–6341
60. Bresser D, Paillard E, Niehoff P, Krueger S, Mueller F, Winter M, Passerini S (2014) Challenges of going nano: enhanced electrochemical performance of cobalt oxide nanoparticles by carbothermal reduction and in situ carbon coating. *Chemphyschem* 15:2177–2185
61. Grugeon S, Laruelle S, Dupont L, Tarascon JM (2003) An update on the reactivity of nanoparticles Co-based compounds towards Li. *Solid State Sci* 5:895–904